

High Temperature Kinetics of the Pyrolysis of 1,3 Butadiene and 2-Butyne

S. Peukert*, M. Braun-Unkhoff, C. Naumann

Deutsches Zentrum für Luft- und Raumfahrt, Institut für Verbrennungstechnik,
Pfaffenwaldring 38-40, 70569 Stuttgart

Abstract

For investigating the pyrolysis of 1,3-butadiene (1,3-C₄H₆) and 2-butyne (2-C₄H₆), reactive gas mixtures highly diluted with argon as bath gas were prepared. The experiments were carried out in a high purity shock tube device over a temperature range of about 1500 – 1800 K at total pressures between 1.2 and 1.9 bar. The time-dependent formation of H-atoms was measured behind reflected shock waves by using the very sensitive method of atomic resonance absorption spectrometry (ARAS). A detailed chemical kinetic reaction mechanism consisting of 33 elementary reactions and 26 species was adapted to model the experimentally obtained H-atom profiles.

Introduction

Practical fuels like diesel, gasoline, and kerosene may consist of blends of numerous species, among them many aliphatic, naphthenic, and aromatic compounds [1-4]. Consequently, the chemical kinetic modelling of their combustion behaviour is a challenging task, due to the complex composition. Therefore, as a prerequisite for simulating a combustion process, a surrogate or model fuel is introduced as a compromise to represent a practical fuel [5]. Surrogates include a limited number of hydrocarbons for which a kinetic reaction model exists that is capable to describe and predict characteristic combustion features like ignition delay time, laminar flame speed, and the formation of pollutants if requested.

For this purpose, one or two compounds from each chemical class (alkane, c-alkanes, alkenes, aromates, ...) are selected to represent the individual chemical classes in a model fuel. To represent the (naphthenic) fuel fraction e.g. in Kerosene, cyclohexane (c-C₆H₁₂) or cyclohexene (c-C₆H₁₀) are mostly chosen as model fuel compounds. Within this context, the chemical kinetics of those compounds expressed by a kinetic sub-model must be known, i.e. to describe the formation of H-atoms correctly, both in rate and amount, over the relevant parameter range. Once, a validated kinetic reaction model exists and is able to predict main characteristic properties, in particular ignition delay time and laminar flame speed, it might be used to simulate combustion processes and thus contributes to the optimization of new sophisticated combustor designs e.g. in engines or gas turbines by numerical simulations using CFD.

1,3-butadiene is expected to be an important intermediate within the thermal decay of cyclohexene which may take place via two initial reaction steps as a competition between C-H and C-C bondage split, respectively; the latter leading to the formation of 1,3-butadiene: $c\text{-C}_6\text{H}_{10} \leftrightarrow \text{C}_2\text{H}_4 + 1,3\text{-C}_4\text{H}_6$ [6-7].

The pyrolysis of 1,3-butadiene has been studied previously in several groups [8-18]. Yet, no consistent picture exists, neither concerning the importance of the nature and the branching ratio of the initiation reactions nor the products formed. For those reasons, a revisited analysis of the 1,3-butadiene system was undertaken in our group, for details, see Peukert *et al.* [19].

Specific Objectives

Two series of shock tube experiments on the pyrolysis of two C₆H₄-isomers, 1,3-butadiene (1,3-C₄H₆) and 2-butyne (2-C₄H₆) were carried out, at similar temperatures and pressures, using very low initial reactant concentrations. The main goal is to describe correctly the production of H-atoms in *both* combustion systems, with the *same* detailed reaction model. The elaborated reaction model comprising 33 reactions and 26 species is capable to match the measured H profiles over the whole investigated parameter range; moreover, it allows also to predict experimental data of main species obtained by Laskin *et al.* [14] studying the pyrolysis of 1,3-butadiene in a plug flow reactor at atmospheric pressure.

Experimental

The shock tube apparatus

All experiments were performed in a stainless steel shock tube of 7.2 cm inner diameter separated by an aluminium diaphragm into a driver and driven section of 4 m and 6.3 m in length, respectively. The apparatus is shown in Fig. 1, for details see ref. [20]. The shock waves were initiated by pressure bursting of the diaphragm using hydrogen as driver gas. The test gas in the low pressure section was argon of high purity with small initial concentrations of 1,3-butadiene (2.0 – 6.0 ppm) or 2-butyne (2.0 – 6.0 ppm).

*Corresponding author: Sebastian.Peukert@dlr.de

Associated Web site: <http://www.dlr.de/VT>

Proceedings of the European Combustion Meeting 2009

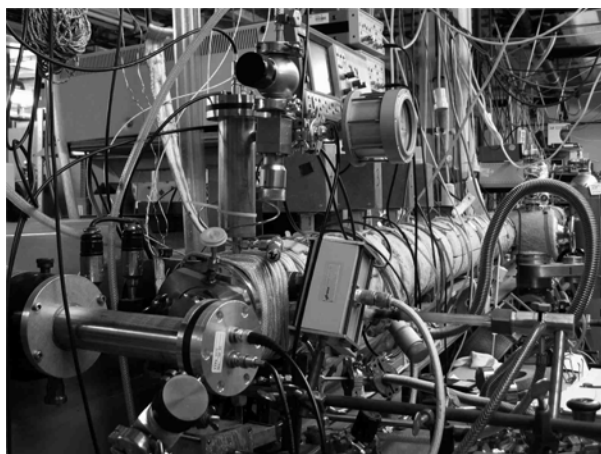


Figure 1. The shock tube seen from the end-flange: Microwave discharge lamps, monochromator (horizontal) and H-ARAS detection (vertical).

Reaction progress was monitored by the detection of H-atoms behind reflected shock waves in a measurement plane 10mm away from the end plate of the tube. H-atom absorption was measured using ARAS at the Lyman α line (121.568 nm) generated by a microwave driven plasma discharge lamp operated with 1% H₂ in He and detected by a solar blind photomultiplier (Thorn EMI / Electron Tubes 9403B). Spectral selectivity was achieved by a combination of a Lyman α interference filter (Acton Research, FWHM = 10 nm) together with an oxygen purge. The experimental observation period was limited to 800 μ s. The storage oscilloscope is triggered by the last of four thin film platinum gauges before the end plate of the tube used to measure the velocity of the incident shock wave. Thus, with the known initial temperature and pressure of the test gas, the state variables of the shock heated test gas mixture (T_s , p_s) behind the reflected shock wave was calculated solving the Rankine-Hugoniot equations and applying the ideal gas law [21].

The test gas mixtures were prepared in a stainless steel vessel heated to 393 K and evacuated to pressures below $1 \cdot 10^{-6}$ mbar. The initial concentrations of the reactants as well as their purity were checked by gas chromatographic analysis (GC-FID).

The purity of the used gases and chemicals were as follows: 1,3-butadiene (Linde) \sim 99.0%, 2-butyne (Sigma-Aldrich) \sim 99.0%, Ar as inert gas (Linde) \sim 99.9999%, H₂ (Linde) as driver gas $>$ 99.8%. For the calibration of H-ARAS a gas mixture (AGA Gas GmbH) was used containing N₂O (2.0 \pm 0.10 ppm), H₂ (207 \pm 10 ppm), rest Ar.

The shock tube was permanently heated to 373 K. Before each series of measurements, H-atom background absorption at Lyman α and temperatures above 2200 K was measured. In our experiments, this background absorption was always below 5% corresponding to an H-atom concentration of $\sim 3 \cdot 10^{11}$ cm⁻³. Thus, we concluded that background effects on the measured H absorption profiles can be ruled out.

The calibration procedure

As mentioned above, the formation of H-atoms was monitored by ARAS at the Lyman α line. The light source is a microwave generated plasma discharge fed by a 1% H₂ in helium gas mixture.

Unfortunately, the correlation between measured absorption and absorber concentration is complicated by the self-reversal of the emission profile at the resonance frequency [22]. Decreasing Doppler broadening of the H-atoms due to temperature gradients along the optical axis of the discharge lamp leads to a resonant absorption of the central line by cooler H-atoms whereas the emitted light from the “spectral wings” of the hottest zone can escape. Because of this complex spectral profile, calibration of the detection system becomes indispensable. We use the well-established reaction sequence starting with N₂O (+ M) \rightarrow N₂ + O (+ M) via H₂ + O \rightarrow OH + H and OH + H₂ \rightarrow H₂O + H to produce H-atoms initialising the reaction system with known concentrations of N₂O and H₂ diluted in Ar [23-24].

The functional relationship between absorber concentration and absorption can be fitted to a modified Lambert-Beer equation:

$$A = 1 - \exp(l \cdot [X]^n \cdot s^{3n-1}) \quad (\text{eq. 1})$$

with A: absorption; l: absorption path length in cm; [X]: concentration of absorber in cm⁻³; for $n = 1$, s^2 corresponds to the classical absorption cross section σ , whereas n is an additional fitting parameter providing a better correlation to $X = X(A)$. Within the temperature range of this investigation, no temperature dependence on the calibration was found.

Results and Discussion

In the present work, a comprehensive study was done on the pyrolysis system of two C₄H₆-isomers, at combustion relevant temperatures and at elevated pressures. For this purpose, two series of experiments were carried out investigating the thermal decomposition of 1,3-butadiene (1,3-C₄H₆) and 2-butyne (2-C₄H₆). Both series were run at similar temperatures and pressures, using very low initial concentrations, to minimize the influence of secondary reactions. The main goal is to describe correctly the rate and the amount of H-atoms formed in *both* reaction systems, by using the *same* reaction model.

It will be shown that the detailed reaction model comprising 33 reactions and 26 species elaborated in the present work (see Table 1) is capable to match the measured H-profiles over the whole investigated parameter range. More over, this reaction model allows also to match species profiles measured by Laskin *et al.* [14] during the pyrolysis of 1,3-butadiene, at atmospheric pressure, see Fig. (8).

Table 1. Reaction model for decomposition of 1,3-butadiene and 2-butyne. Reaction coefficient: $k = A T^n \exp(-E_{act}/RT)$; units cm, s, mol, cal. Values for E_{act} are given in $\text{cal}\cdot\text{mol}^{-1}$; *: + Ar; #: (+M)

No.	Reaction	A	n	E_{act}	Ref.
R 1	$2\text{-C}_4\text{H}_6 \leftrightarrow 2\text{-C}_4\text{H}_5 + \text{H}$	$3.8 \cdot 10^{15}$	0.0	89200	<i>p.w.</i>
R 2	$2\text{-C}_4\text{H}_6 \leftrightarrow 1,2\text{-C}_4\text{H}_6$	$6.9 \cdot 10^{13}$	0.0	64600	<i>p.w.</i>
R 3	$1,3\text{-C}_4\text{H}_6 \leftrightarrow \text{C}_2\text{H}_2 + \text{C}_2\text{H}_4$	$7.0 \cdot 10^{12}$	0.0	67100	<i>p.w.</i>
R 4	$2\text{-C}_4\text{H}_6 \leftrightarrow 1,3\text{-C}_4\text{H}_6$	$3.0 \cdot 10^{13}$	0.0	65000	[15]
R 5	$1,2\text{-C}_4\text{H}_6 \leftrightarrow 1,3\text{-C}_4\text{H}_6$	$2.5 \cdot 10^{13}$	0.0	63000	[15]
R-6	$2 \text{C}_2\text{H}_3 \leftrightarrow 1,3\text{-C}_4\text{H}_6$	$1.5 \cdot 10^{42}$	-8.8	12483	[30]
R7#	$\text{C}_2\text{H}_3 \leftrightarrow \text{C}_2\text{H}_2 + \text{H}$ k_∞ k_0 TROE $a = 1.982$	$3.9 \cdot 10^8$ $2.6 \cdot 10^{27}$ $T^{***} = 5383.7, T^* = 4.3$	1.62	37048 -3.40 35799	[31]
R 8	$1,3\text{-C}_4\text{H}_6 \leftrightarrow \text{C}_4\text{H}_4 + \text{H}_2$	$2.5 \cdot 10^{15}$	0.0	94700	[15]
R 9	$1,3\text{-C}_4\text{H}_6 \leftrightarrow i\text{-C}_4\text{H}_5 + \text{H}$	$5.7 \cdot 10^{36}$	-6.3	112353	[30]
R 10	$1,3\text{-C}_4\text{H}_6 \leftrightarrow n\text{-C}_4\text{H}_5 + \text{H}$	$5.3 \cdot 10^{44}$	-8.6	123608	[30]
R11#	$\text{C}_3\text{H}_3 + \text{CH}_3 \leftrightarrow 1,2\text{-C}_4\text{H}_6$ k_∞ k_0 TROE $a = 0.175$	$1.5 \cdot 10^{12}$ $2.6 \cdot 10^{57}$ $T^{***} = 1340.6; T^* = 60000$ $T^{**} = 9769.8$	0.0	0 -11.9 9770	[30]
R 12	$\text{C}_3\text{H}_3 \leftrightarrow \text{C}_3\text{H}_2 + \text{H}$	$7.65 \cdot 10^{12}$	0.0	78365	[33]
R 13	$2 \text{C}_3\text{H}_3 \leftrightarrow \text{phenyl} + \text{H}$	$3.0 \cdot 10^{11}$	0.0	0	[33]
R 14	$2 \text{C}_3\text{H}_3 \leftrightarrow \text{benzene}$	$6.5 \cdot 10^{12}$	0.0	0	[33]
R 15	$1\text{-C}_4\text{H}_6 \leftrightarrow 1,2\text{-C}_4\text{H}_6$	$2.5 \cdot 10^{13}$	0.0	65000	[16]
R 16	$1\text{-C}_4\text{H}_6 \leftrightarrow \text{C}_3\text{H}_3 + \text{CH}_3$	$3.0 \cdot 10^{15}$	0.0	75800	[16]
R 17	$1,2\text{-C}_4\text{H}_6 \leftrightarrow i\text{-C}_4\text{H}_5 + \text{H}$	$4.2 \cdot 10^{15}$	0.0	92600	[32]
R 18	$2\text{-C}_4\text{H}_5 \leftrightarrow i\text{-C}_4\text{H}_5$	$5.0 \cdot 10^{12}$	0.0	50500	[34]
R 19	$2\text{-C}_4\text{H}_5 \leftrightarrow t\text{-C}_4\text{H}_4 + \text{H}$	$6.0 \cdot 10^{13}$	0.0	53000	[34]
R 20	$t\text{-C}_4\text{H}_4 + \text{H} \leftrightarrow \text{H}_2 + i\text{-C}_4\text{H}_3$	$3.0 \cdot 10^7$	2.0	6000	[34]
R21*	$\text{C}_2\text{H}_4 \leftrightarrow \text{C}_2\text{H}_3 + \text{H}$	$2.6 \cdot 10^{17}$	0.0	96512	[35]
R22*	$\text{CH}_3 \leftrightarrow \text{CH} + \text{H}_2$	$3.1 \cdot 10^{15}$	0.0	80836	[36]
R23*	$\text{CH}_3 \leftrightarrow \text{CH}_2 + \text{H}$	$2.2 \cdot 10^{15}$	0.0	82624	[36]
R 24	$2 \text{CH}_3 \leftrightarrow \text{C}_2\text{H}_5 + \text{H}$	$3.0 \cdot 10^{13}$	0.0	13506	[37]
R 25	$\text{C}_2\text{H}_5 \leftrightarrow \text{C}_2\text{H}_4 + \text{H}$	$8.2 \cdot 10^{12}$	0.0	39895	[35]
R 26	$\text{C}_4\text{H}_4 \leftrightarrow \text{C}_2\text{H}_2 + \text{C}_2\text{H}_2$	$3.4 \cdot 10^{13}$	0.0	77102	[38]
R 27	$\text{C}_4\text{H}_4 \leftrightarrow \text{C}_4\text{H}_2 + \text{H}_2$	$1.3 \cdot 10^{15}$	0.0	94680	[38]
R28*	$\text{C}_4\text{H}_4 \leftrightarrow n\text{-C}_4\text{H}_3 + \text{H}$	$1.1 \cdot 10^{20}$	0.0	99109	[38]
R 29	$\text{C}_4\text{H}_2 + \text{H} \leftrightarrow n\text{-C}_4\text{H}_3$	$1.1 \cdot 10^{42}$	-8.7	15300	[30]
R 30	$\text{C}_4\text{H}_4 + \text{H} \leftrightarrow n\text{-C}_4\text{H}_5$	$1.3 \cdot 10^{51}$	-11.9	16500	[30]
R 31	$\text{C}_4\text{H}_4 + \text{H} \leftrightarrow i\text{-C}_4\text{H}_5$	$4.9 \cdot 10^{51}$	-11.9	17700	[30]
R 32	$n\text{-C}_4\text{H}_3 + \text{H} \leftrightarrow \text{C}_4\text{H}_4$	$2.0 \cdot 10^{47}$	-10.3	13070	[39]
R 33	$i\text{-C}_4\text{H}_3 + \text{H} \leftrightarrow \text{C}_4\text{H}_4$	$3.4 \cdot 10^{43}$	-9.0	12120	[39]

Modelling procedure and thermodynamics

For modelling the measured H-atom absorption time profiles, an adaptation of the SENKIN code of the CHEMKIN II programme suite was used [26]. If not otherwise stated, the rate of each elementary reaction was computed for both directions; those of the reverse reaction were obtained from the k-values of the forward reaction and the equilibrium constant. If available, the species' thermodynamic properties (see Table 2) were mostly taken from ref. [27]; otherwise from [28].

Table 2. Heat of formation values of important species used in the present work, mostly taken from Wang [27]. Values are given in kcal mol^{-1} .

Species	$\Delta H_{f, 298}^0$
1,3-C ₄ H ₆ (1,3-butadiene)	26.3
1,2-C ₄ H ₆ (1,2-butadiene)	39.3
2-C ₄ H ₆ (2-butyne)	34.7
1-C ₄ H ₆ (1-butyne)	39.5 [28]
C ₄ H ₄ (vinyl acetylene)	68.0
C ₂ H ₂ (acetylene)	54.5
C ₂ H ₄ (ethylene)	12.6
n-C ₄ H ₅ (2-butene-1-yl)	85.4
i-C ₄ H ₅ (2-butene-2-yl)	77.4
C ₃ H ₃ (propargyl radical)	82.7
CH ₃ (methyl radical)	35.1
C ₂ H ₃ (vinyl radical)	71.6

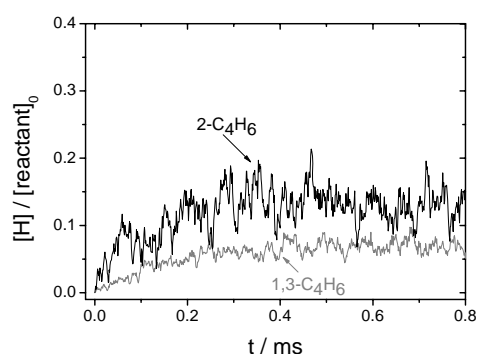


Fig. 2. Comparison of $[\text{H}]/[\text{reactant}]_0$ -ratio measured for two C₄H₆-isomers: $T_5 = 1603 \text{ K}$, $p_5 = 1.91 \text{ bar}$.

Comparing H profiles measured in both systems

A typical experimental H-atom-profile is displayed in Fig. 2, for both investigated reactants, normalized to the initial reactant concentration. According to this figure, the thermal decomposition of 2-C₄H₆ yields a larger amount of H-atoms compared to the one of 1,3-butadiene, at similar conditions (temperature, pressure, initial concentration). For 1,3-butadiene, this ratio is smaller over the whole temperature range covered by the measurements. In the case of 2-butyne as reactant, more H-atoms will be produced at lower temperatures compared to 1,3-butadiene.

If the pyrolysis process started with 2-butyne as reactant, then reaction (R 1) $2\text{-C}_4\text{H}_6 \leftrightarrow 2\text{-C}_4\text{H}_5 + \text{H}$ is the initial reaction step directly producing H-atoms. On the other hand, if the pyrolysis process is started with 1,3-butadiene as reactant, reaction (R 1) is a subsequent reaction occurring only after the 1,3-butadiene has undergone isomerisation to 1,2-C₄H₆ and 2-butyne according to the reverse reaction (R 5) $1,2\text{-C}_4\text{H}_6 \leftrightarrow 1,3\text{-C}_4\text{H}_6$ and reaction (R 2) $1,2\text{-C}_4\text{H}_6 \leftrightarrow 2\text{-C}_4\text{H}_6$. The most stable thermodynamic isomer is 1,3-butadiene; hence, the chemical equilibrium of the isomerisation reactions (R 5) $1,2\text{-C}_4\text{H}_6 \leftrightarrow 1,3\text{-C}_4\text{H}_6$ and (R 4) $2\text{-C}_4\text{H}_6 \leftrightarrow 1,3\text{-C}_4\text{H}_6$ is on the right hand side. For those reasons, a time delay and a lower level in the formation of H-atoms is observed during the pyrolysis of 1,3-butadiene compared to the pyrolysis of 2-butyne.

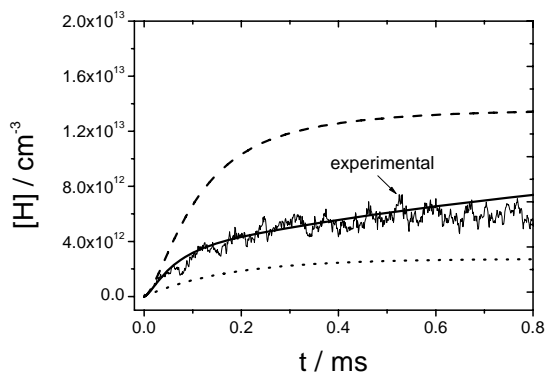


Figure 3. Comparison between measured and computed H-atom profile using different reaction models: 5.4 ppm 1,3-C₄H₆, balance Ar, $T_5 = 1661$ K, $p_5 = 1.78$ bar. Solid curve: reaction model, *p. w.*; dotted curve: reaction model, Rao *et al.* [12]; dashed curve: reaction model, Laskin *et al.* [14].

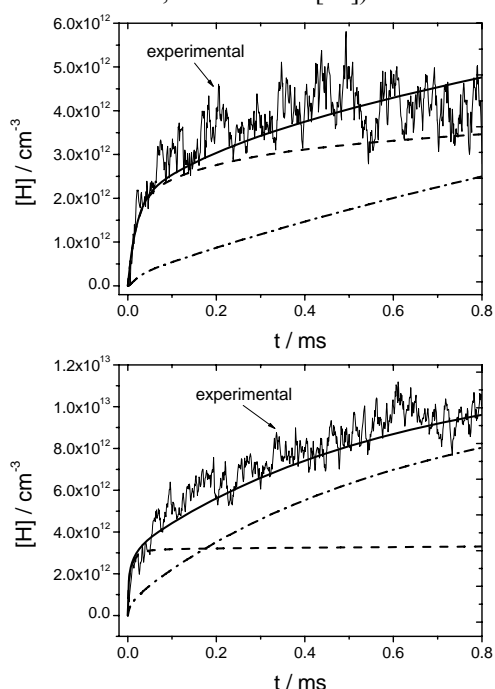


Figure 4: Influence of reactions (R 1) and (R 12) on H atom production. Solid curve: full model; dashed curve: without (R 12); dash-dotted curve: without (R 1). Top: $T_5 = 1579$ K, $p_5 = 1.91$ bar, 2.4 ppm 2-C₄H₆, balance Ar. Bottom: $T_5 = 1770$ K, $p_5 = 1.92$ bar, 2.0 ppm 2-C₄H₆, balance Ar.

Modelling of H profiles with results of former studies

Presently, no comprehensive understanding about the branching ratio and the reaction rate expressions of the several initiation steps of 1,3-butadiene reaction system exists, see refs. [8]–[18]. 1,3-butadiene may decompose via different initial reaction steps, as a competition between C-H and C-C bondage split. This may be attributed to the existence of further C₄H₆-isomers, with 2-butyne and 1,2-butadiene among them: 2-C₄H₆ ↔ 1,3-C₄H₆ (R 4) and 1,2-C₄H₆ ↔ 1,3-C₄H₆ (R 5).

Using the detailed kinetic reaction model of the present work (see Table 1), H-atom profiles obtained within the pyrolysis of 1,3-butadiene and 2-butyne,

respectively, were reproduced (see Fig. 3, solid curves). On the other hand, the reaction model published by Laskin *et al.* [14] underrates the measured H-atom profile (Fig. 3, dotted curves), whereas the one given by Rao *et al.* [12] overrates the measured H-atom profiles, in particular at the early stage of the investigated time interval (Fig. 3, dashed curve).

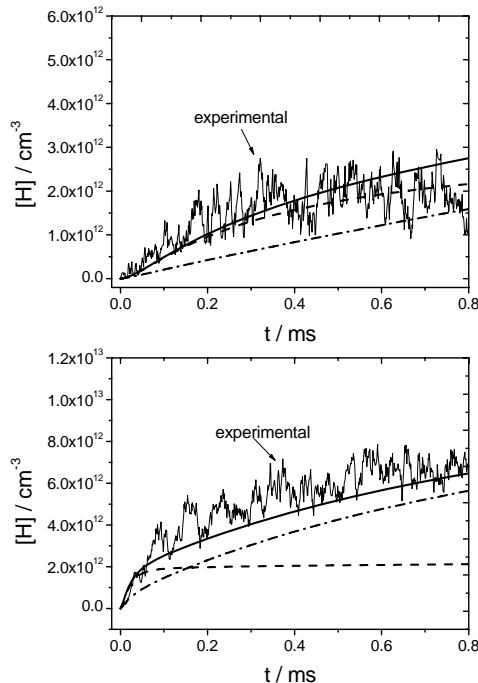


Figure 5: Influence of reactions (R 1) and (R 12) on H atom production. Solid curve: full model; dashed curve: without (R 12); dash-dotted curve: without (R 1). Top: $T_5 = 1547$ K, $p_5 = 1.94$ bar, 6.0 ppm 1,3-C₄H₆, balance Ar. Bottom: $T_5 = 1736$ K, $p_5 = 1.82$ bar, 2.7 ppm 1,3-C₄H₆, balance Ar.

Modelling 1,3-butadiene and 2-butyne experiments

Perturbation sensitivity plots indicate that the isomerisation reaction (R 2) 2-C₄H₆ ↔ 1,2-C₄H₆ has a much larger influence on the H-atom formation for the 2-butyne system compared to the 1,3-butadiene system [19]. By performing kinetic modelling for reaction (R 2) it was possible to describe *all* experimental data. Over the investigated temperature range of the experiments carried out in the present work, the values for (R 2) had to be modified by up to a factor of 4. This adaptation was necessary in order to describe *both* the 1,3-butadiene and 2-butyne experiments consistently.

Additionally, the rate coefficient of reaction (R 1) had to be modified slightly compared to the values given in ref. [15].

Importance of reaction (R 3): 1,3-C₄H₆ ↔ C₂H₂ + C₂H₄

The products of the molecular channel (R 3) are ethylene and acetylene. For temperatures below 2000 K, both species are very stable, and do not decompose in notable amounts. Although reaction (R 3) does not contribute directly to the formation of H-atoms, it affects the H-atom profiles indirectly: The faster this reaction channel proceeds, the less the other H-

contributing reactions steps will be attended. On the other hand, with respect to the thermal decomposition of 2-butyne, reaction (R 3) has only a minor influence on H-atom formation.

For the reproduction of the 1,3-butadiene *and* the 2-butyne experiments, kinetic modelling of the molecular channel (R 3) was performed. The values of the rate coefficient obtained for reaction (R 3) are plotted in Fig. 6 (solid curve) as a function of temperature. For comparison, Arrhenius expressions published in literature are shown as well and plotted within the investigated temperature range (dotted curve: Tsang *et al.* [13]; dashed curve: Laskin *et al.* [14]).

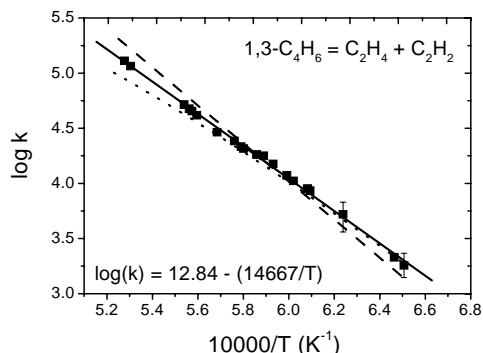


Fig. 6: Arrhenius plot for reaction (R 3): $1,3\text{-C}_4\text{H}_6 \leftrightarrow \text{C}_2\text{H}_4 + \text{C}_2\text{H}_2$. Symbols & solid curve: *p. w.*; dashed curve: Laskin *et al.* [14]; dotted curve: Tsang [13].

The Arrhenius expression obtained by Tsang *et al.* [13] as a result of a master equation analysis is given by $k(T)/\text{s}^{-1} = 4.2 \cdot 10^{88} \cdot T^{20.85} \cdot \exp(132873 [\text{cal} \cdot \text{mol}^{-1}]/RT)$. At temperatures between 1500 and 1900 K, the determined rate coefficient values of the present work are in good compliance. Also, again, good agreement is found between the rate coefficient values obtained in the present work and those reported by Laskin *et al.* [14] when extrapolating their rate coefficients to the temperature range of the present work.

Importance of reaction (R 1): $2\text{-C}_4\text{H}_6 \leftrightarrow 2\text{-C}_4\text{H}_5 + \text{H}$

In principle, we could have also tried to describe the 1,3-butadiene pyrolysis experiments by modelling reaction (R-1). However, if the Arrhenius equation of reaction (R 1) would have been strongly modified as it would have been necessary considering the 1,3-butadiene experiments *alone*, then we would not have been able to reproduce the H-atom profiles measured during the thermal decomposition of 2-butyne. Additionally, it should be mentioned that the Arrhenius equation for the decomposition of propargyl radicals according to (R 12) that turned out to have an important impact on the amount of H-concentration profiles (see e.g. Fig. 5) was not changed at all, as this reaction was investigated in an experimental H-ARAS shock tube study by Scherer [33] under conditions comparable to those of the present experiments.

All derived values for the rate coefficient of reaction (R 1) are plotted in Fig. 7 (symbols, solid curve). For comparison, the Arrhenius expression published by Hidaka *et al.* [15] resulting from quantum RRKM

calculations is given as well for the temperature range covered by the experiments of the present work.

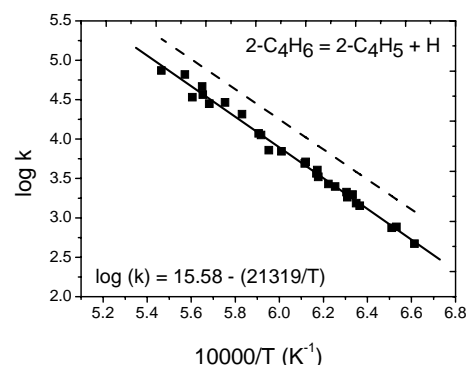


Fig. 7: Arrhenius plot for reaction (R 1): $2\text{-C}_4\text{H}_6 \leftrightarrow 2\text{-C}_4\text{H}_5 + \text{H}$. Solid curve, symbols: *p. w.*; dashed curve: Hidaka *et al.* [15].

Modelling 1,3-butadiene or 2-butyne experiments

If the 1,3-butadiene experiments have been modelled *separately*, *without* consideration of the experimental set of 2-butyne, it would be possible to match the H-atom profiles measured during the thermal decay of 1,3-butadiene by the reaction model shown in Table 1, with one exception: for reactions (R1) $2\text{-C}_4\text{H}_6 \leftrightarrow 2\text{-C}_4\text{H}_5 + \text{H}$ and (R 2) $1,2\text{-C}_4\text{H}_6 \leftrightarrow 2\text{-C}_4\text{H}_6$, Arrhenius expressions had to be adjusted to those given by Hidaka *et al.* [15]. However, this adjusted reaction model – with the modified Arrhenius parameters for (R1) and (R 2) – would then predict a much higher rate of H-atom formation if the 2-butyne experiments would be modelled *separately*, *without* consideration of the experimental set of 1,3-butadiene. Furthermore, a successful description of the 2-butyne experiments with these modified reaction rates for (R 1) and (R 2) would not be possible. Reaction (R 3) $1,3\text{-C}_4\text{H}_6 \leftrightarrow \text{C}_2\text{H}_4 + \text{C}_2\text{H}_2$ does not contribute directly to the production of H-atoms below temperatures of 2000 K although it is an important initial reaction step for the thermal decay of 1,3-butadiene.

Now the other way round: Reproducing the 2-butyne experiments by kinetic modelling *separately*, *without* consideration of the experimental set of 1,3-butadiene, the values for the rate coefficient of reaction (R 1) had to be modified slightly, in order to be consistent with the 1,3-butadiene dataset, although (R 1) is the most important reaction in the 2-butyne system according to the perturbation sensitivity analysis.

Thus, further reactions had to be considered. The isomerisation reaction (R 4) $2\text{-C}_4\text{H}_6 \leftrightarrow 1,3\text{-C}_4\text{H}_6$ has some influence on the predicted H-concentration profiles for both systems, 1,3-butadiene and 2-butyne. In order to describe the 2-butyne experiments, it would be necessary to adapt the rate coefficient values for (R 4) extensively, by up to a factor of 5, but then it would not be possible to describe *both* experimental datasets, with the *same* reaction model and the *same* set of Arrhenius parameters any more.

Check of the elaborated reaction model

As a check of the reaction model derived in the present work (Table 1), further simulations were done using experiments reported by Laskin *et al.* [14]. A comparison of calculated and measured species profiles of 1,3-butadiene and 1,2-butyne are shown in Fig. 8; for further components, see Peukert *et al.* [19]. Overall, very good agreement was found despite the different temperature regimes of the two experimental studies.

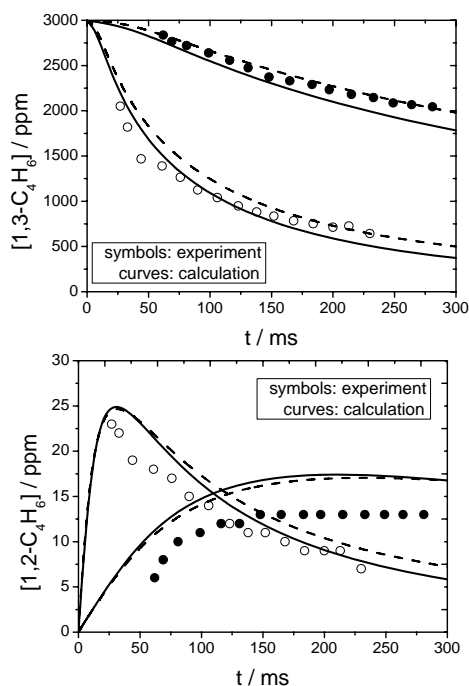


Fig. 8: Measured (symbols, Laskin *et al.* [14]) and computed (curves) species profiles. 3000 ppm 1,3-butadiene in N_2 ; $p = 1$ atm; $T = 1110$ K (open circles) and $T = 1185$ K (full circle). Dashed curve: reaction model & rate coefficients by Laskin *et al.*; solid curve: reaction model by Laskin *et al.*, rate coefficients: *p. w.*

Conclusions

The thermal decomposition of 1,3-butadiene ($1,3-C_4H_6$) and 2-butyne ($2-C_4H_6$), respectively, was investigated in a high purity shock tube device over a temperature range of about 1500 – 1800 K at total pressures between 1.2 and 1.9 bar, highly diluted with argon. The formation of H-atoms was measured as a function of time behind reflected shock waves by using the very sensitive ARAS technique. By modelling *both* sets of experimental data *simultaneously* and applying sensitivity and reaction flux analysis, a detailed chemical kinetic reaction mechanism with 33 elementary reactions and 26 species was generated. This reaction model was proven to match the experimentally obtained H-atom profiles and to comply with experiments by Laskin *et al.* at much lower temperature.

Acknowledgements

The authors like to thank N. Ackermann for his help with the analysis procedure. Furthermore, S.P. is thankful for funding within the Collaborative Research

Centre 606 “Non-stationary Combustion: Transport Phenomena, Chemical Reactions, Technical Systems”

References

1. Dagaut, P., *Phys. Chem. Chem. Phys.* 4 (2002), 2079-94.
2. Dean, A. J., Penyazkov, O. G., Sevruck, K. L., Varatharajan, B.: *Proc. Comb. Inst.* 30 (2007), 2481-88.
3. Steil, U., Braun-Unkloff, M., Frank, P., Aigner, M.: Paper no 973, 46th AIAA Aerospace Sciences Meeting 7- 10 Jan 2008 (USA).
4. Slavinskaya, N.: Paper 0992, 46th AIAA Aerospace Sciences Meeting and Exhibit 7-10 Jan 2008, Reno, USA
5. Wahl, C., Kapernaum, M.: EU-project CFD4C, final report, project no. GRDI-1999-10325 (2001).
6. Dayma, G.; Fournet, G. R.; Battin-LeClerc F.: *Int. J. Chem. Kinet.* 35 (2003) 273.
7. Steil, U., Braun-Unkloff, M., Naumann, C., Frank, P.: European Combustion Meeting, Louvain la Neuve (Belgium), (2005).
8. Skinner, G.B.; Sokolowski, E.M.: *J. Phys. Chem.* 64 (1960) 1028.
9. Benson, S. W.; Haugen, G. R.: *J. Phys. Chem.* 71 (1967) 1735.
10. Kiefer, J.H.; Wei, H.C.; Kern, R.D.; Wu, C.H.: *Int. J. Chem. Kinet.* 17 (1985) 225.
11. Kiefer, J.H.; Mitchell, K.I.; Wei, H.C.: *Int. J. Chem. Kinet.* 20 (1988) 787.
12. Rao, V.S.; Takeda, K.; Skinner, G.B.: *Int. J. Chem. Kinet.* 20 (1988) 153
13. Tsang, W.; Mokrushin, V.: *Proc. Comb. Inst.* 28 (2000) 1717.
14. Laskin, A.; Wang, H.; Law, C.K.: *Int. J. Chem. Kinet.* 32 (2000) 589
15. Hidaka, Y.; Higashihara, T.; Ninomiya, N.; Masaoka, H.; Nakamura, T.; Kawano, H.: *Int. J. Chem. Kinet.* 28 (1996) 137.
16. Hidaka, Y.; Higashihara, T.; Ninomiya, N.; Oshita H.; Kawano, H.: *J. Phys. Chem.* 97 (1993) 10977.
17. Hidaka, Y.; Higashihara, T.; Ninomiya, N.; Oki, T.; Kawano, H.: *Int. J. Chem. Kinet.* 27 (1995) 331.
18. Chambreau, S. D.; Lemieux, J.; Wang, L.; Zhang, J.: *J. Phys. Chem. A* 109 (2005) 2190.
19. Peukert S., Braun-Unkloff M., Naumann C., *Z. Physik. Chem.* 2008 accepted
20. Xu, C., Braun-Unkloff, M., Naumann, C., Frank, P.: *Proc. Combust. Inst.* 31 (2007) pp. 231 – 239.
21. Wright, J. K.: Shock Tubes. Methuen & Co Ltd, UK (1961).
22. Tsang, W.; Lifshitz, A.: *Ann. Rev. Phys. Chem.* 41 (1990) 559.
23. Just, Th. in Shock waves in chemistry, (Lifshitz, A.) M. Dekker, New York (1981) 279.
24. Masten, D. A.; Hanson, R. K.; Bowman, C. T.: *J. Phys. Chem.* 94 (1990) 7119.
25. Frank, P.; Just, Th.: *Ber. Bunsenges. Phys. Chem.* 89 (1985) 181.
26. Lutz, A. E., Kee, R. J. Miller, J. A., SENKIN: Sandia National Laboratories, Livermore, CA, USA 94551-0969, report SAND87-8248, Feb. (1988).
27. Wang, H., University of California at Los Angeles (USA) 2000. <http://ignis.usc.edu/Mechanisms/C4H6/c4h6.html>
28. Burcat A., Technion Institute Haifa, Israel (2007); <ftp://ftp.technion.ac.il/pub/supported/aetdd/thermodynamics>,
29. Benson, S. W.: Thermochemical Kinetics. John Wiley & Sons, USA (1976).
30. Wang, H.; Frenklach, M.: *Comb. Flame* 110 (1997) 173.
31. Knyazev, V. D.; Slagle, I. R.: *J. Phys. Chem.* 100 (1996) 16899.
32. Leung, K. M.; Linstedt, R. P.: *Comb. Flame* 102 (1995) 129.
33. Scherer, S.; Ph.D. Thesis, University of Stuttgart, (2001).
34. Belmekki, N., Glaude, P. A., Da Costa, I., Fournet, R., Battin-Leclerc, F.: *Int. J. Chem. Kinet.* 34 (2002) 172.
35. Baulch, D. L.; Cobos, C. J.; Cox, R. A.; Frank, P.; Hayman, G.; Just, Th.; Kerr, J. A.; Murrells, T.; Pilling, M. J.; Troe, J.; Walker, R. W.; Warnatz, J.: *J. Phys. Chem. Ref. Data* 23 (1994) 847.
36. Venkatesh, V.; Hanson, R.K.; Golden, D.M., Bowman, C.T.; Davidson, D. F.: *J. Phys. Chem. A* 111 (2007) 4062
37. Baulch, D.L.; Cobos, C. J.; Cox, R.A.; Esser, C.; Frank, P.; Just, Th.; Kerr, J. A.; Pilling, M. J.; Troe, J.; Walker, R. W.; Warnatz, J.: *J. Phys. Chem. Ref. Data* 21 (1992) 411
38. Braun-Unkloff, M.; Kurz, A.; Frank, P.: *Proc. 17th Intern. Symp. on Shock Waves* (1989) 493.
39. Wang, H., Ph.D thesis, The Pennsylvania State University, University Park, PA, (1992)